Applied Surface Science 532 (2020) 147369

Contents lists available at ScienceDirect

Applied Surface Science

journal homepage: www.elsevier.com/locate/apsusc

Correlation between surface chemistry and morphology of PtCu and Pt nanoparticles during oxidation-reduction cycle

Maria Kalyva[a,*], Martin F. Sunding[b], Annette E. Gunnæs[c], Spyros Diplas[b], Evgeniy A. Redekop[a]

[a] Centre for Materials Science and Nanotechnology (SMN), Department of Chemistry, University of Oslo, POBox 1033 Blindern, N-0315 Oslo, Norway
[b] Materials Physics Oslo, SINTEF Industry, Forskningsveien 1, NO - 0373 Oslo, Norway
[c] Structure Physics, Department of Physics, University of Oslo, Forskningsparken-Oslo Innovation Center, FERMiO Gaustadalleen, 210349 Oslo, Norway

ARTICLE INFO

Keywords:
Microwave synthesis
Bimetallic nanocatalysts
Surface chemistry
Structure
Redox

ABSTRACT

Process conditions during catalytic reactions induce significant changes in surface chemistry and structure of bi-(mono) metallic nanoparticles leading to their deactivation, and this can ultimately affect the reactions long-term performance. Here PtCu and Pt model nanoparticles are prepared by microwave synthesis and characterized by X-ray diffraction (XRD). Surface chemical and morphological changes of the nanoparticles during high-temperature oxidation and reduction treatments cycle are correlated by near *in situ* X-ray photoelectron spectroscopy (XPS) and *ex situ* transmission electron microscopy (TEM) - energy-dispersive X-ray spectroscopy (EDS) studies. At 300 °C the surface atomic composition of the PtCu nanoparticles switches reversibly upon the cycle and at the same time their morphology and composition are maintained. At 400 °C, the surface atomic composition does not fully restore and, while the shape is maintained, the size and composition are not. This occurs by a mechanism of Cu leaching out from the nanoparticles. These data delineate potential operating conditions for stable PtCu nanocatalysts.

1. Introduction

Nanocatalysts have emerged as a new class of materials, since they exhibit superior properties for a range of catalytic processes as compared to their bulk counterparts [1]. Bimetallic nanoparticles (NPs) have drawn considerable interest for a number of catalytic applications, such as oxidation and reduction reactions, environmental catalysis (CO and NOx oxidation), fuel cells and energy storage, because they exhibit higher catalytic efficiencies than the monometallic nanoparticles. The enhanced properties are due to the potential synergy between the metals [2]. Nanocatalysts participating in heterogeneous catalytic processes usually encounter harsh reaction environments, such as gases and high temperatures which are responsible for their deactivation. The primary routes of deactivation are through poisoning, coarsening and/or volatilization under gas phase reaction conditions [3]. As a result, nanocatalysts may change their surface chemistry, morphology, and chemical composition under reaction conditions [4]. In bimetallic nanocatalysts reaction gases and/or temperature effects could induce interdiffusion between the two components and even changes of the chemical state of the metals. As such, complex dynamic processes are expected to occur in the bimetallic nanocatalyst systems under reaction conditions. Correlating the surface chemical state with the structure of the nanocatalysts by controlling the process conditions, so as to prevent or slow down catalyst deactivation, is of great importance towards designing stable catalysts for long-term reaction performances.

Alloying Pt with nonprecious metals such as, Cu can play a critical role in modifying its electronic properties, for example the surface Pt *d*-band. The average energy of the *d*-band has been correlated to the adsorption energy of atoms and small molecules on transition metal surfaces, and thus to predicting catalytic performance [5]. Adding nonprecious metals to Pt decreases the amount of the noble metal and therefore cost when preparing nanocatalysts [6]. Platinum-copper (PtCu) bimetallic NPs have been demonstrated as active heterogeneous catalysts for a range of scientifically and industrially important reactions, such as NO reduction with hydrogen [7], liquid phase hydrogenation of acrylonitrile to acrylamide and of 1,3-cyclooctadiene to cyclooctene [8], propane dehydrogenation [9], and oxygen reduction reaction. [10].

PtCu bimetallic NPs with small particle size ($\leq$9 nm) and narrow size distributions have been synthesized for catalytic applications mainly by chemical routes, such as the one-pot hydrothermal method [11], co-reduction of platinum and copper precursors [12], modified polyol process [8] and co-reduction of the precursors using a combination of surfactants and solvents [13]. These methods require long

* Corresponding author.
E-mail address: m.e.kalyva@smn.uio.no (M. Kalyva).

https://doi.org/10.1016/j.apsusc.2020.147369
Received 23 April 2020; Received in revised form 16 July 2020; Accepted 24 July 2020
Available online 29 July 2020

reaction times (e.g., couple of hours to a day), specific environmental conditions (e.g., gas atmospheres (argon, nitrogen), high temperatures and pressures, etc.), hazardous reagents and careful quenching of the reactions. Microwave dielectric heating is a relatively new synthesis route that has several advantages compared to chemical routes, including shorter reaction times, reduced energy consumption, and higher yields, and as such is considered a 'green' nanosynthesis method [14]. PtCu NPs have been previously synthesized for catalytic applications using a conventional microwave oven within 2 min, but with poor size distribution [15]. Monodispresed 5 nm distribution required a 12 h mixing process before the short microwaves reaction [16]. Recently, supported PtCu alloy nanocatalysts of 3.7 nm were prepared in 10 min by microwave-assisted polyol method using a scientific microwave oven, but the Pt to Cu content could not be controlled [17].

Herein we report the rapid synthesis of bimetallic PtCu (13 min) and monometallic Pt NPs (5 min) with sizes $<$ 10 nm using a scientific microwave oven, the low-toxicity ethylene glycol as solvent and non-toxic polyvinylpyrrolidone (PVP) polymer as capping agent. PtCu and Pt NPs were drop casted onto SiO_2 wafers and exposed to near *in-situ* oxidation and reduction cycle at 300 °C and 400 °C. XPS spectra were recorded at the end of each process in order to investigate the chemical and compositional changes occurring on the surfaces of the NPs. The results were correlated with changes in morphology and composition of the NPs, under similar conditions, studied by TEM-EDS.

2. Experimental

2.1. Chemicals and Materials

Platinum(IV) chloride ($PtCl_4$, +99.9%), Copper(II) acetylacetonate ($Cu(acac)_2$, 99.99%), Oleylamine (OAm, tech. 70%), Polyvinylpyrrolidone (PVP, 10 000), and Ethylene glycol (EG, 99.8%) were purchased from Sigma–Aldrich.

2.2. Synthesis of PtCu, Pt and Cu NPs

In a typical synthesis, for the preparation of PtCu nanoparticles (NPs), equimolar ratio of the metallic precursors were dissolved in EG (10 mL) and then mixed with OAm (5 mL) and PVP. For the monometallic NPs only the corresponding metallic precursor was mixed into the solution. Then, the solution was placed in a microwave oven of MicroSYNTH T640 pro-24 of Milestone Srl., operating up to 1000 Watts, 200 °C and 30 bar. The oven is equipped with a thermocouple, to follow the temperature in the reaction solution, and a continuous stirring base. The reaction was performed at 200 °C for 13 min. Preparation of the Pt NPs was performed in a similar reaction for 5 min, using only the corresponding metallic precursor. After cooling down slowly in air, the nanocrystals were obtained by flocculating the reaction solution in ethanol, followed by particle separation using a centrifuge operating at 5000 rpm for 5 min. The particles were washed at least two times with ethanol/hexane mixture before re-dispersing in hexane (10 mL).

2.3. Characterization of NPs

Powder X-ray diffraction (XRD) patterns were collected at room temperature with a Bruker D8 Discover diffractometer equipped with a Ge(111) monochromator, which gave CuKα radiation (λ = 1.5406 nm) and a position-sensitive LynxEye detector. The free-standing NPs were deposited on specially cut Si single-crystal zero-background holders. High-resolution transmission electron microscopy (HRTEM) images were acquired with a JEOL JEM-2100F microscope operating at 200 kV and equipped with a Gatan Orius SC 200D2, 14 bit, 11 meg-apixel CCD and a spherical aberration corrector in the objective lens to ensure a point resolution of 1.2 Å. NPs were deposited onto Ni-grids, and 150 particles of PtCu and Pt were measured to prepare histograms. An Oxford Inca energy-dispersive silicon-drift X-ray (EDS), X-MaxN80 T spectrometer was used for the compositional analysis.

2.4. XPS measurements of the NPs

XPS spectra were collected before and after exposure of PtCu and Pt NPs on SiO_2 surfaces, separately, to ~10 mol.% O_2 in Ar at 1 bar at 300°C and 400°C for 30 min. The temperatures were typically reached within ~15 min and after that no C 1s signal was observed in XPS. Subsequently, the surface was exposed to ~3 mol.% H_2 in Ar at 1 bar at the same conditions. The binding energy (BE) scale was calibrated using the Si^0 2p peak at 99.3 eV of the NP substrate. The high temperature oxidation and reduction cycles were performed in an adjacent reaction cell attached to the XPS instrument, were by the samples can be transferred without breaking vacuum between their treatments and surface analysis (near *in-situ*). XPS analysis of the samples was performed with a Kratos Axis Ultra DLD instrument by using monochromatic AlKα radiation ($h\nu$ = 1486.6 eV) at 15 kV and 10 mA. The pass energies for the survey and high-resolution scan were 160 and 20 eV, respectively. The XPS atomic ratios were calculated using the integrated peak areas of $Pt4f_{7/2}$ and $Cu2p_{3/2}$ and their relative sensitivity factors. The pressure in the chamber was maintained below of 6×10^{-9} Torr during the analysis.

3. Results and discussion

The synthesized bimetallic PtCu NPs appear to be spherical, having an average NP size (D) of (7.0 ± 0.7) nm as shown by the histogram originating from the TEM images analysis and "near-monodisperse" distribution with coefficient of variation (CV) ≤ 0.15, (i.e. CV = σ/D, in which σ and D are the standard deviation and mean size, respectively) [18], (Fig. 1a). High-resolution TEM (HRTEM) of single PtCu nanoparticles (Fig. 1b) shows clear lattice fringes with an interfringe distance *d*-spacing of 1.876 Å, as measured from the corresponding Fourier-transform (FT) pattern. This *d*-spacing corresponds to the lattice spacing of alloy Pt–Cu {200} planes with a close-packed structure (cps) [19]. TEM-EDS analysis shows a 49:51 (in at.%) Pt:Cu composition of the NPs, (Fig. 1c), similar to the starting nominal composition of the precursors. The synthesized monometallic Pt NPs appear to have non-uniform shapes, having an average NP size (D) of (8.7 ± 1.3) nm and "near-monodisperse" distribution (Fig. 1d). High-resolution TEM (HRTEM) of single Pt nanoparticles shows clear lattice fringes (Fig. 1e) with interfringe distance *d*-spacing of 1.930 Å as measured from the corresponding Fourier-transform (FT) pattern (Fig. 1f), which corresponds to the lattice spacing of Pt {020} planes with close-packed structure (cps). [20]

Powder X-ray diffraction (XRD) patterns, revealed the crystalline nature of the PtCu and Pt NPs (Fig. 2). Pt NPs present strong diffraction peaks at 2θ ≈ 39.9, 46.4, and 67.6° and 81.5°, (Fig. 2b) that can be indexed to the (111), (200), (220) and (311) planes of face-centered cubic (fcc) of pure platinum. [21] PtCu NPs present diffraction peaks at higher values 2θ ≈ 41.2°, 47.9°,70.3°and 84.67°, (Fig. 2a) indicating that alloying is taking place that can be indexed to the (111), (200), (220) and (311) planes of fcc platinum-copper phase [22].

The PtCu NPs pattern appears to be very broad and asymmetric compared to the Pt NPs pattern, which could originate from a significant rearrangement of the atoms at the surface of the particle, the presence of defects as well as strain and/or disorder in the crystal structure [23]. The crystallite size and lattice parameter values of the PtCu and Pt NPs were calculated by fitting the patterns with TOPAS software, while for the PtCu NPs pattern the strain parameter in TOPAS analysis was included in our calculations. The lattice parameters values of the Pt and PtCu NPs are found to be 3.9160(1) and 3.7837(1) Å respectively, in agreement with reported values for Pt and Pt-50 at.% Cu NPs [24,25]. The crystallite size values for the Pt and PtCu NPs are found to be 8.1 nm and 6.0 nm, close and relatively smaller to the

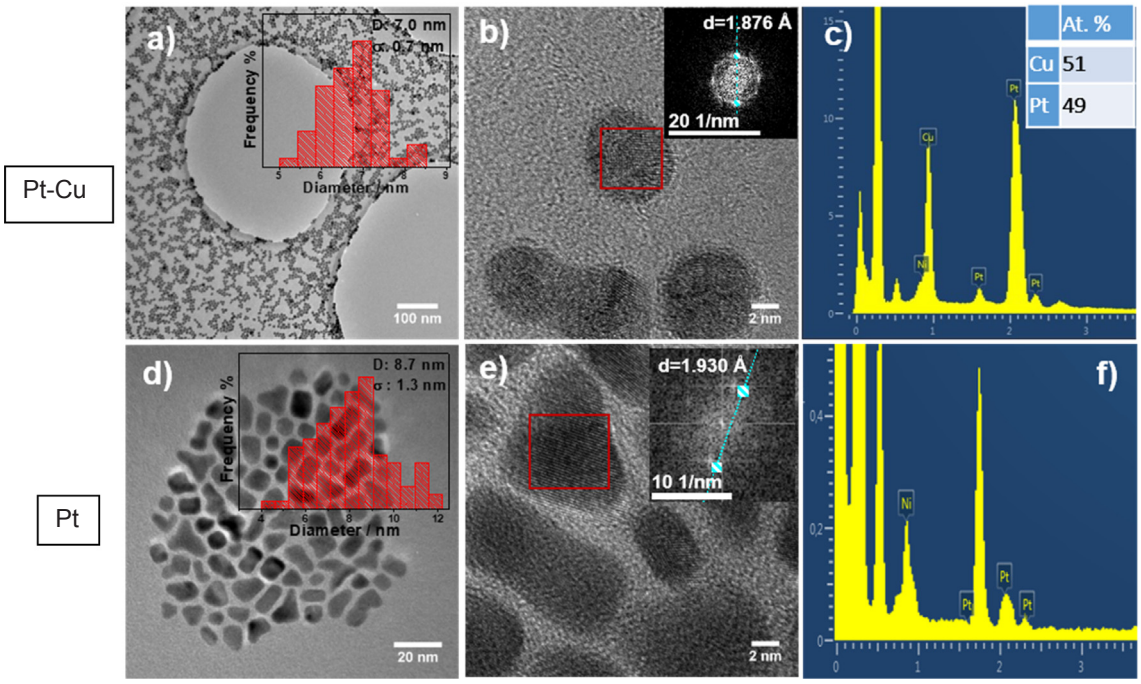

Fig. 1. TEM images (inset: histogram) (a), (d), HRTEM images (inset: FFT pattern of a single NP) (b), (e) and HRTEM-EDS spectra (c), (f) of PtCu and Pt NPs correspondingly.

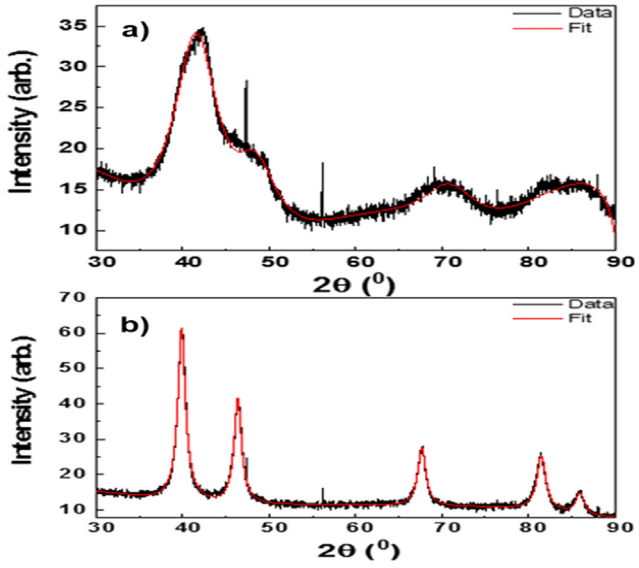

Fig. 2. Powder XRD patterns of a) PtCu and b) Pt NPs with Si-reference.

average particle size shown with TEM respectively. Rearrangement of the atoms at the surface of the particle, contribution from defects, strain or/and disorder, usually has as result that the XRD size analysis gives smaller value than TEM [26]. To further support our analysis, we used the Williamson and Hall (W-H) model, which differentiates between size- and strain-induced peak broadening and we calculated the NPs size to be 5.8 nm in good agreement with TOPAS results, SI [27].

The XPS $Pt4f_{7/2}$ and $Cu2p_{3/2}$ peaks of the as-prepared PtCu NPs, are found at BEs characteristic of metallic Pt and Cu respectively (Fig. 3a and b, Table 1) [28,29]. After Oxidation at 300 °C the XPS $Pt4f_{7/2}$ peak is shifting to higher BE, but the shift is too small to be assigned to PtO oxide (BE range 71.7–72.0 eV) (Fig. 3a, Table 1). [30] This difference in the BE from the as-prepared sample could be ascribed to the effects of surface restructuring which has previously been observed for Pt-based NPs, especially pronounced upon the first redox cycle [31,32]. The broad shoulder on the higher BE side of the main Pt doublet corresponds to Cu 3p electrons. Similarly, the XPS Cu $2p_{3/2}$ peak is found at higher BE, and a strong shake-up feature at 942.6 eV appears, suggesting the formation of CuO oxide (Fig. 3b, Table 1) [11]. Subsequent reduction shifts the $Pt4f_{7/2}$ and $Cu2p_{3/2}$ peaks to lower BEs with simultaneous disappearing of the Cu shake-up peaks. This can be assigned to the formation of metallic Pt and Cu states, respectively. Therefore, the chemical state of Cu reversibly switches between Cu^{2+} and Cu^0, while Pt changes are more subtle indicating that Pt remains essentially metallic during the treatments. The XPS $Pt4f_{7/2}$ peak originating from the Pt NPs is found at BE characteristic of metallic Pt (Fig. 3c, Table 1). After oxidation and reduction at 300 °C, the XPS $Pt4f_{7/2}$ peak shifts slightly to higher and lower BEs, respectively, but in the BE range typical for metallic Pt.

The XPS Pt 4f BE of Pt NPs appears at lower BE with respect to that of PtCu NPs, implying a change in the electronic structure of Pt upon the formation of alloy with Cu. The BE shift is not in agreement with the trend expected from the electronegativities of Pt and Cu, which would imply a charge transfer from Cu to Pt. The apparent difference in the NPs BEs can be attributed to quantum confinement effects [33]. Assuming equal shifts of all energy levels the Pt 3d center shifts away from the Fermi level for Pt in the Pt-Cu NPs as compared to pure Pt NPs. Due to the downshift of the Pt d-band center in PtCu alloy catalyst, the adsorption energy of the intermediate species reduces, thus enhancing the catalytic activity for relevant reactions, such as, the methanol oxidation reaction [34].

Interestingly, the XPS intensity of the Pt 4f and Cu 2p signals of the bimetallic PtCu NPs varies significantly with the oxidation and reduction treatments. Upon oxidation the Cu 2p peak area increases and simultaneously the Pt 4f decreases, while upon reduction the opposite is observed. This reversible behavior can be clearly demonstrated by plotting the surface atomic ratio (at.%) of Pt and Cu when alternating exposures in experimental cycle (Fig. 3d).

The observed changes in XPS Pt and Cu intensities from the PtCu particles during oxidation and reduction cycles can be attributed to surface restructuring. It has been shown previously that the adsorption of oxygen on Pt–Cu catalyst surfaces could induce segregation of 3d transition metal onto the top surface, owing to strong bonding between

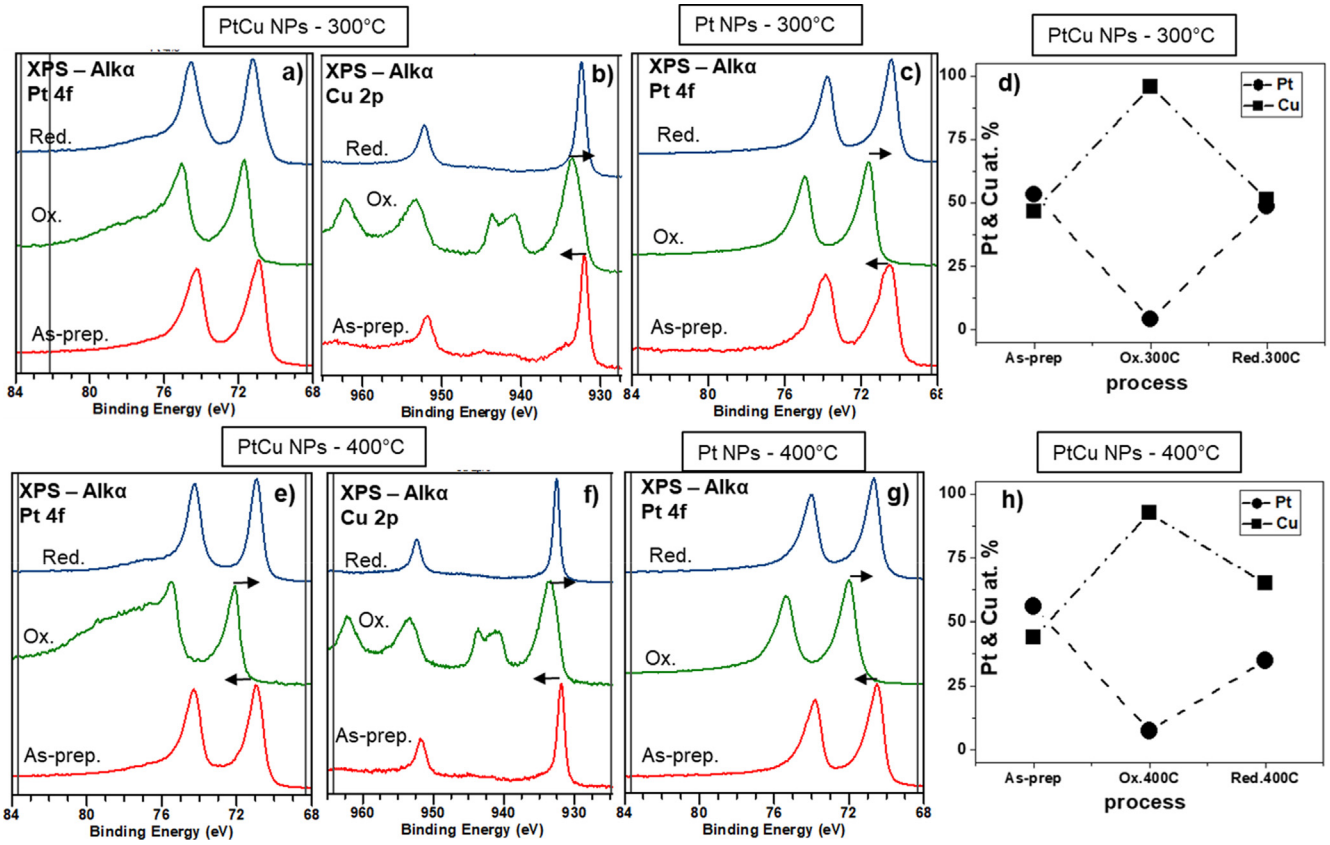

Fig. 3. XPS spectra from PtCu and Pt NPs deposited on SiO_2 substrates in oxidation-reduction cycle reactions at 300 °C (a), (b), (c) and 400 °C (e), (f), (g). Surface atomic ratio of PtCu NPs in oxidation-reduction cycle reactions having at.% standard errors of 3% or below (calculated from repeating experiments for all the processes) at 300 °C d) and 400 °C h).

oxygen and 3d transition metals [35]. The 3d transition metal oxide CuO formed at 300 °C (Fig. 3b) tends to encapsulate Pt, since most oxides have low surface energy (< 1 J/m^2) [36] compared to that of Pt (surface energy of Pt: 1.95 J/m^2 [37]). Therefore, upon oxidation the XPS Pt intensity is decreasing and Cu increasing. Surface segregation of Pt has been found in vacuum in PtCu bimetallic systems, where the metal with larger atomic radius (Pt:1.39 Å, Cu:1.28 Å) segregates to the surface in order to release strain at the bimetallic surface [38,39]. Since hydrogen bonds weakly to most 3d transition metals, the presence of H_2 will not change the thermodynamic driving force for the surface segregation process. Therefore, upon reduction Pt segregates to the surface, restoring the surface Pt:Cu atomic ratio.

After cycle of oxidation and reduction of PtCu NPs at 400 °C, XPS measurements show the reversible chemical switch of the chemical state of Cu ($Cu^{2+} \rightarrow Cu^0$) and Pt ($Pt^{2+} \rightarrow Pt^0$) (Fig. 3e and g, Table 1). The surface chemical state of Pt indicates alteration between the oxidized and the metallic state during the treatments. However, the chemical state of Pt remains metallic during the treatments at 300 °C, reflecting the possibility of a different catalytic response. At alternating oxidation and reduction treatments at 400 °C of Pt NPs, the chemical state of Pt reversibly switches between Pt^{2+} and Pt^0 during the experimental cycle. (Fig. 3g, Table 1). At 400 °C the surface atomic ratio (at.%) of Pt and Cu, reversibly alternates upon the exposures, but the composition does not fully restore, as at 300 °C.

The Pt $4f_{7/2}$ BE shifts (Table 1). To higher BE in the Pt-Cu system than in pure Pt. Although the shifts are marginal (close or within the experimental error), they show that Pt core holes are not as efficiently screened in the Pt-Cu environment as in pure Pt. At 400 °C cycle the shifts are smaller (almost negligible), and this might be related to a decrease of the number of Cu neighbors around Pt atoms. At 300 °C, Cu reversibly diffuses onto the surface, leaving a Pt rich underlayer and back to the core, but at 400 °C the process seems to be less reversible resulting in a permanent compositional change.

The morphology of Pt NPs does not seem to change after oxidation and after reduction both at 300 °C and 400 °C, SI (Figure A). XPS shows that the oxide species on the surface of the NPs is assigned to PtO and not PtO_2, the latter being a volatile oxide as has been shown earlier [40]. TEM-EDS analysis shows that after the 300 °C oxidation the

Table 1
XPS BEs and Pt$4f_{7/2}$ BE shifts between PtCu and Pt NPs as-prepared, after Oxidation and Reduction cycle at 300 °C and 400 °C.

State of NPs	Pt$4f_{7/2}$BE ± 0.2(eV)[a] **PtCu** NPs	Cu$2p_{3/2}$BE ± 0.3(eV)[a] **PtCu** NPs	Pt$4f_{7/2}$ BE ± 0.2(eV)[a] **Pt** NPs	Pt$4f_{7/2}$ BE shift ± 0.28(eV)[a] between **PtCu** & **Pt** NPs
As-prep.	70.9	932.1	70.5	0.4
Ox. 300 °C	71.6	933.7	71.1	0.5
Reduc.300 °C	71.2	932.4	70.4	0.8
Ox. 400 °C	72.1	934.3	72	0.1
Reduc. 400 °C	71	932.4	70.7	0.3

[a] Casa XPS software, version 2.3.18. PR1.0.

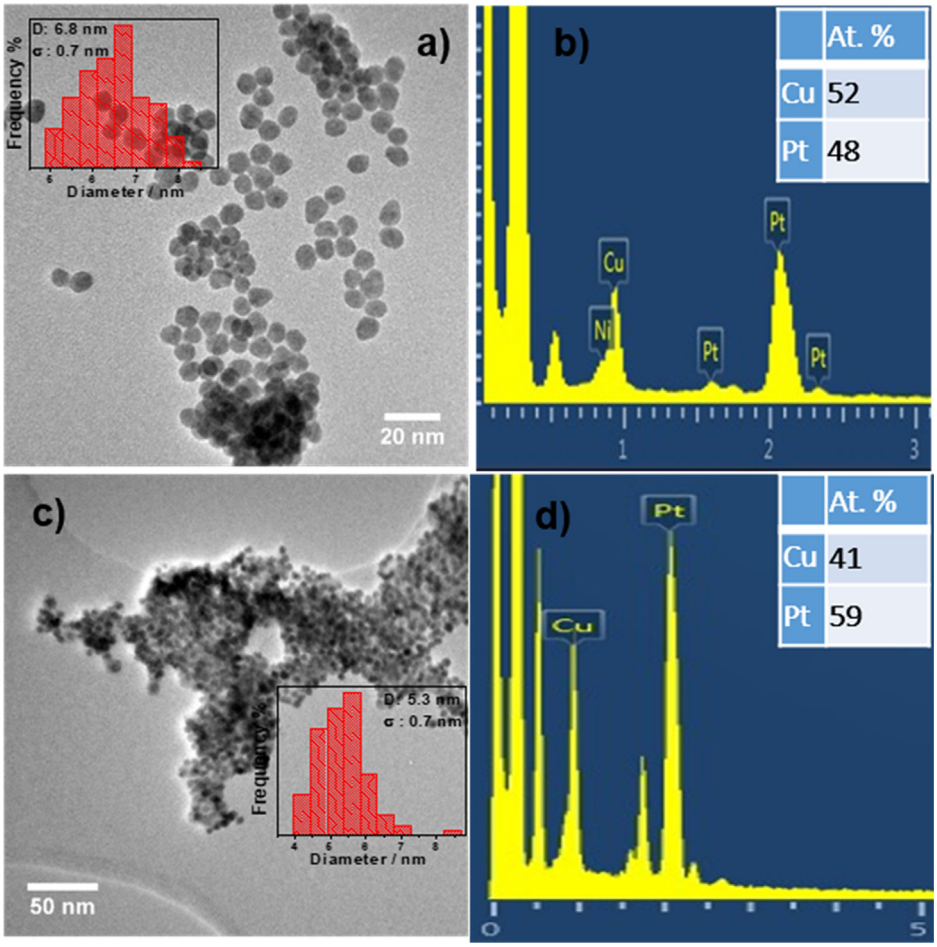

Fig. 4. TEM images (inset: histogram) (a), (c) and TEM-EDS spectra (b), (d), of PtCu NPs after oxidation at 300 °C and 400 °C.

average size, shape and composition of the PtCu NPs does not change (Fig. 4a and b). After reduction at 300 °C the morphology and composition of the NPs does not change. Thus, at these conditions, the surface atomic composition (XPS) of the NPs is reversible, while their morphology is preserved.

This is not the case at higher temperatures, as at 400 °C oxidation TEM-EDS analysis shows that even though the NPs shape remains spherical, their average size decreases to ~ 5 nm and the composition Pt:Cu changes to ~ 60:40 at.% (Fig. 4c and d). The increase of the Pt content of the PtCu NPs is explained by a leaching out mechanism [41] of Cu, since smaller (1–4 nm) Cu NPs are detected, SI (Figure B). After reduction the morphology and composition of the NPs remain the same as after oxidation. At 500 °C oxidation, the processing conditions seem to be harsh that the NPs coalesce, SI (Figure C).

4. Conclusion

In conclusion, we have prepared well-dispersed PtCu and Pt nanoparticles by a novel microwave-based synthesis route and investigated their segregation/alloying behavior under oxidation-reduction cycle at elevated temperatures. XPS analysis of supported PtCu nanoparticles onto SiO_2 at 300 °C shows that surface chemical state of Cu ($Cu^{2+} \leftrightarrow Cu^0$) changes reversibly, Pt (Pt^0) remains almost metallic and the surface atomic composition switches reversibly upon the cycle. At the same time, TEM-EDS analysis suggests that the NPs morphology and composition does not change. At 400 °C, the chemical state of both Cu ($Cu^{2+} \leftrightarrow Cu^0$) and Pt ($Pt^{2+} \leftrightarrow Pt^0$) reversibly switches, but the surface atomic composition does not fully restore. TEM-EDS analysis show that shape is maintained but not the size and chemical composition, by Cu leaching out from the PtCu nanoparticles. At higher temperature (500 °C), the morphology is not maintained. These observations will pave the way for optimizing the operating conditions for stable PtCu nanocatalysts in technological applications.

CRediT authorship contribution statement

Maria Kalyva: Conceptualization, Methodology, Investigation, Data curation, Writing - original draft. **Martin F. Sunding:** . **Annette E. Gunnæs:** . **Spyros Diplas:** . **Evgeniy A. Redekop:** .

Declaration of Competing Interest

The authors declare that they have no known competing financial interests or personal relationships that could have appeared to influence the work reported in this paper.

Acknowledgements

Research leading to these results received funding from the Research Council of Norway (#272266, TAPXPS project). The authors acknowledge the use of the Norwegian national research infrastructures including the National Surface And Interface Characterisation Laboratory (NICE) and the Norwegian Centre for Transmission Electron Microscopy (NORTEM). The authors would also like to express their gratitude to Prof. Unni Olsbye of the University of Oslo for her support.

Appendix A. Supplementary data

Supplementary data to this article can be found online at https://doi.org/10.1016/j.apsusc.2020.147369.

References

[1] P. Serp, K. Philippot, Nanomaterials in Catalysis, in: D. Astruc (Ed.) Wiley-VCH, Weinheim (2013) pp. 496.
[2] S.B. Singh, P.K. Tandon, Catalysis: a brief review on nano-catalyst, J. Energy Chem. Eng. 2 (3) (2014) 106–115.
[3] P. Forzatti, L. Lietti, Catalyst deactivation, Catal. Today 52 (1999) 165–181.
[4] H. Tanaka, M. Uenishi, M. Taniguchi, I. Tan, K. Narita, M. Kimura, K. Kaneko, Y. Nishihata, J. Mizuki, The intelligent catalyst having the self-regenerative function of Pd, Rh and Pt for automotive emissions control, Catal. Today 17 (2006) 321.
[5] P. Strasser, S. Koh, T. Anniyev, J. Greeley, K. More, C.F. Yu, Z.C. Liu, S. Kaya, D. Nordlund, H. Ogasawara, M.F. Toney, A. Nilsson, Lattice-strain control of the activity in dealloyed core–shell fuel cell catalysts, Nat. Chem. 2 (2010) 454–460.
[6] D.L. Wang, H.L.L. Xin, R. Hovden, H.S. Wang, Y.C. Yu, D.A. Muller, F.J. DiSalvo, H.D. Abruna, Structurally Ordered Intermetallic Platinum − Cobalt Core − Shell Nanoparticles with Enhanced Activity and Stability as Oxygen Reduction Electrocatalysts, Nat. Mater. 12 (2012) 81–87.
[7] A. Obuchi, A. Ogata, K. Mizuno, A. Ohi, H. Ohuchi, Properties of Pd@Au and Pt@Cu alloy surfaces for the adsorption and catalytic reduction of O2 and NO by H2, Colloids Surf. A 80 (1993) 121–126.
[8] N. Toshima, Y. Wang, Preparation and catalysis of novel colloidal dispersions of copper/noble metal bimetallic clusters, Langmuir 10 (1994) 4574–4580.
[9] Z. Ma, Z. Wu, J.T. Miller, Effect of Cu content on the bimetallic Pt–Cu catalysts for propane dehydrogenation, Catal. Struct. React. 3 (2017) 43–53.
[10] G.W. Sievers, J.R. Bowen, V. Brüser, M. Arenz, Support-free nanostructured PtCu electrocatalyst for the oxygen reduction reaction prepared by alternating magnetron sputtering, J. Power Sources 413 (2019) 432–440.
[11] X. Du, S. Luo, H. Du, M. Tang, X. Huang, P.K. Shen, Monodisperse and self-assembled Pt-Cu nanoparticles as an efficient electrocatalyst for the methanol oxidation reaction, J. Mater. Chem. A 4 (2016) 1579.
[12] M. Gao, W. Yang, Y. Yu, Monodisperse PtCu alloy nanoparticles as highly efficient catalysts for the hydrolytic dehydrogenation of ammonia borane, Int. J. of Hydrogen Energy 43 (2018) 14293–14300.
[13] D. Xu, Z. Liu, H. Yang, Q. Liu, J. Zhang, Jiye Fang, S. Zou, and K. Sun, Solution-based evolution and enhanced methanol oxidation activity of monodisperse platinum–copper nanocubes, Angew. Chem. Int. Ed. 48 (2009) 4217–4221.
[14] J.A. Dahl, B.L.S. Maddux, J.E. Hutchison, Toward greener nanosynthesis, Chem. Rev. 107 (2007) 2228.
[15] V. Abdelsayed, A. Aljarash, M. Samy El-Shall, Z.A. Al Othman, A.H. Alghamdi, Microwave synthesis of bimetallic nanoalloys and CO oxidation on ceria-supported nanoalloys, Chem. Mater. 21 (2009) 2825.
[16] X. Peng, D. Chen, X. Yang, D. Wang, M. Li, C.-C. Tseng, R. Panneerselvam, X. Wang, W. Hu, J. Tian, Y. Zhao, Microwave-Assisted Synthesis of Highly Dispersed PtCu Nanoparticles on Three-Dimensional Nitrogen-Doped Graphene Networks with Remarkably Enhanced Methanol Electrooxidation, ACS Appl. Mater. Interfaces 8 (2016) 33673–33680.
[17] H. El-Deeb, M. Bron, Microwave-assisted polyol synthesis of PtCu/carbon nanotube catalysts for electrocatalytic oxygen reduction, J. Power Sources 275 (2015) 893–900.
[18] M. Kalyva, D.S. Wragg, H. Fjellvåg, A.O. Sjåstad, Engineering Functions into Platinum and Platinum-Rhodium Nanoparticles in a One-Step Microwave Irradiation Synthesis, ChemistryOpen 6 (2017) 273–281.
[19] G. Saravanan, R. Khobragade, L.C. Nagara, N. Labhsetwar, Ordered intermetallic Pt–Cu nanoparticles for the catalytic CO oxidation reaction, RSC Adv. 6 (2016) 85634.
[20] R. Esparza, G. Rosas, E. Valenzuela, S.A. Gamboa, U. Pal, R. Pérez, Structural analysis and shape-dependent catalytic activity of Au, Pt and Au/Pt nanoparticles, Revista Matéria 13 (2008) 579–586.
[21] G. Gao, G. Yang, M. Xu, C. Wang, C. Xu, H. Li, Simple synthesis of Pt nanoparticles on noncovalent functional MWNT surfaces: Application in ethanol electrocatalysis, J. Power Sources 173 (2007) 178–182.
[22] R. Lamber, S. Wetjen, N.I. Jaeger, Size dependence of the lattice parameter of small palladium particles, Phys. Rev. B 51 (1995) 10968.
[23] B. Ingham, X-ray scattering characterisation of nanoparticles, Crystallogr. Rev. 21 (2015) 229–303.
[24] Y. Jia, J. Su, Z. Chen, K. Tan, Q. Chen, Z. Cao, Y. Jiang, Z. Xie, L. Zheng, Composition-tunable synthesis of Pt–Cu octahedral alloy nanocrystals from PtCu to PtCu3via underpotential-deposition-like process and their electro-catalytic properties, RSC Adv. 5 (2015) 18153–18158.
[25] P. Müller, U. Hejral, U. Rütt, A. Stierle, In situ oxidation study of Pd–Rh nanoparticles on MgAl 2 O 4 (001), Phys. Chem. Chem. Phys. 16 (2014) 13866.
[26] B. Akbari, M. Pirhadi Tavandashti, M. Zandrahimi, Particle size characterization of nanoparticles – a practical approach, Iran. J. Mater. Sci. Eng. 8 (2) (2011) 48–56.
[27] Y.T. Prabhu, K.V. Rao, V.S.S. Kumar, B.S. Kumari, X-ray analysis by Williamson-Hall and size-strain plot methods of ZnO nanoparticles with fuel variation, World J. Nano Sci. Eng. 4 (2014) 21–28.
[28] L.K. Ono, B. Yuan, H. Heinrich, B. Roldan Cuenya, Formation and thermal stability of platinum oxides on size-selected platinum nanoparticles: support effects, J. Phys. Chem. C 114 (2010) 22119–22133.
[29] J.F. Moulder, W.F. Stickle, P.E. Sobol, K.D. Bomben, Handbook of XPS Spectra, Perkin-Elmer Corporation, Physical Electronics Division, 1992.
[30] L.K. Ono, J.R. Croy, H. Heinrich, B. Roldan Cuenya, Oxygen Chemisorption, Formation, and Thermal Stability of Pt Oxides on Pt Nanoparticles Supported on SiO2/Si(001): Size Effects, J. Phys. Chem. C 115 (2011) 16856–16866.
[31] M. Filez, H. Poelman, E.A. Redekop, V.V. Galvita, K. Alexopoulos, M. Meledina, R.K. Ramachandran, J. Dendooven, C. Detavernier, G. Van Tendeloo, O.V. Safonova, M. Nachtegaal, B.M. Weckhuysen, G.B. Marin, Kinetics of Lifetime Changes in Bimetallic Nanocatalysts Revealed by Quick X-ray Absorption Spectroscopy, Angew. Chem. Int. Ed. 57 (2018) 12430–12434.
[32] F. Tao, M.E. Grass, Y. Zhang, D.R. Butcher, J.R. Renzas, Z. Liu, Jen Y. Chung, B.S. Mun, M. Salmeron, G.A. Somorjai, Reaction-Driven Restructuring of Rh-Pd and Pt-Pd Core-Shell Nanoparticles, Science 322 (2008) 932–934.
[33] I. Aruna, B.R. Mehta, L.K. Malhotra, S.M. Shivaprasad, Size dependence of core and valence binding energies in Pd nanoparticles: Interplay of quantum confinement and coordination reduction, J. Appl. Phys. 104 (2008) 064308.
[34] W. Kang, R. Li, D. Wei, S. Xu, S. Wei, H. Li, CTAB-reduced synthesis of urchin-like Pt–Cu alloy nanostructures and catalysis study towards the methanol oxidation reaction, RSC Adv. 5 (2015) 94210–94215.
[35] C.A. Menning, H.H. Hwu, J.G. Chen, Experimental and theoretical investigation of the stability of Pt − 3d − Pt (111) bimetallic surfaces under oxygen environment, J. Phys. Chem. B 110 (2006) 15471.
[36] D. Chatain, I. Rivollet, N. Eustathopoulos, Adhésion thermodynamique dans les systèmes non-réactifs métal liquide-alumine, J. Chim. Phys. 83 (1986) 561.
[37] D. Sander, H. Ibach, Landolt-Bornstein—Group III Condensed Matter/42A2, (Eds. Springer), (2002).
[38] J. Knudsen, A.U. Nilekar, R.T. Vang, J. Schnadt, E.L. Kunkes, J.A. Dumesic, M. Mavrikakis, F. Besenbacher, A Cu/Pt Near-Surface Alloy for Water − Gas Shift Catalysis, J. Am. Chem. Soc. 129 (2007) 6485.
[39] J.A. Dean, Lange's Handbook of Chemistry, 15th ed., McGraw-Hill, 1999.
[40] P. Wynblatt, N.A. Gjostein, Supported metal crystallites, Prog. Solid State Chem. 9 (1975) 21–58.
[41] A. Cao, G. Veser, Exceptional high-temperature stability through distillation-like self- stabilization in bimetallic nanoparticles, Nat. Mater. 9 (2010) 75–81.